## Observation of Anisotropic Superfluid Density in an Artificial Crystal

J. Taoo, \* M. Zhaoo, \* and I. B. Spielmano

Joint Quantum Institute, University of Maryland and National Institute of Standards and Technology, College Park, Maryland 20742, USA

(Received 21 December 2022; accepted 7 August 2023; published 18 October 2023)

We experimentally and theoretically investigate the anisotropic speed of sound of an atomic superfluid (SF) Bose-Einstein condensate in a 1D optical lattice. Because the speed of sound derives from the SF density, this implies that the SF density is itself anisotropic. We find that the speed of sound is decreased by the optical lattice, and the SF density is concomitantly reduced. This reduction is accompanied by the appearance of a zero entropy normal fluid in the purely Bose condensed phase. The reduction in SF density—first predicted [A. J. Leggett, Phys. Rev. Lett. 25, 1543 (1970).] in the context of supersolidity—results from the coexistence of superfluidity and density modulations, but is agnostic about the origin of the modulations. We additionally measure the moment of inertia of the system in a scissors mode experiment, demonstrating the existence of rotational flow. As such we shed light on some supersolid properties using imposed, rather than spontaneously formed, density order.

DOI: 10.1103/PhysRevLett.131.163401

Superfluidity and Bose-Einstein condensation (BEC) are deeply connected. In dilute atomic BECs, the superfluid (SF) and condensate densities are generally equal [1,2]. By contrast, SF <sup>4</sup>He can achieve nearly 100% SF fraction, with only about 14% condensate fraction [3], and infinite 2D Berezinski-Kosterlitz-Thouless (BKT) SFs have no condensate at all [4,5]. In 1970 Tony Leggett showed that supersolids—systems spontaneously forming both SF and crystalline order (i.e., density modulations)—exhibit the reverse behavior: SF density far below the condensate density [6]. Here we observe this effect in a nearly pure atomic BEC with artificial crystalline order imprinted by an optical lattice.

The complex-valued order parameter [7]  $\phi(\mathbf{r}) = \sqrt{\rho^{\rm sf}} \exp[i\varphi(\mathbf{r})]$ , describing an SF with number density  $\rho^{\rm sf}$  and phase  $\varphi(\mathbf{r})$ , gives rise to two hallmark SF properties: dissipationless supercurrents associated with spatial gradients in  $\varphi(\mathbf{r})$  and (Bogoliubov [2]) phonons described by traveling waves in  $\varphi(\mathbf{r})$ . Because dissipationless supercurrents—both electrical, and as here, neutral—arise from phase gradients, they are locally irrotational; in liquid <sup>4</sup>He, the resulting nonclassical rotational inertia [8,9] appears below the SF transition temperature  $T_{\rm c}$ . Supersolids are more exotic systems spontaneously forming crystalline order while exhibiting SF transport properties and phase coherence [10]. Recent experiments with dipolar BECs of Dy and

Published by the American Physical Society under the terms of the Creative Commons Attribution 4.0 International license. Further distribution of this work must maintain attribution to the author(s) and the published article's title, journal citation, and DOI. Er exhibit crystalline order and phase coherence [11–13], suggestive of SF. Leggett argued that the modulated density  $\rho(\mathbf{r})$  of a supersolid leads to an unavoidable reduction in  $\rho^{\rm sf}$ , and derived an upper bound for  $\rho^{\rm sf}$  [6]. This reduction is accompanied with the appearance of an unusual normal fluid, that is pinned to the lattice potential and contrary to the usual two-fluid model carries no entropy. Here the reduced superfluid density results from the 3D density distribution, and as such is masked in tight binding descriptions such as the Bose-Hubbard model, which makes the unrelated prediction of vanishing  $\rho^{\rm sf}$  at the superfluid to Mott insulator transition [14,15].

We created an artificial SF crystal by imprinting periodic density modulations into an atomic BEC using a 1D optical lattice as in Fig. 1(a). While these modulations do not form spontaneously, Leggett's result still applies, making this an ideal system for understanding crystalline SFs without the added complexity of spontaneously broken symmetries. We experimentally measured an anisotropic speed of sound via Bragg spectroscopy [16] of the phonon mode. This implies the existence of an effective anisotropic superfluid density—which can be expressed as a second rank tensor  $\rho_{ij}^{\rm sf}$ —and we find that it saturates Leggett's bound, in agreement with Gross-Pitaveskii equation (GPE) simulations. We also obtained an associated modification to the moment of inertia from measurements of the scissors-mode frequencies [17,18].

Anisotropic superfluids.—Here we consider pure 3D BECs well described by the Gross-Pitaveskii wave function  $\psi(\mathbf{r}) = |\psi(\mathbf{r})| \exp[i\vartheta(\mathbf{r})]$ . An optical lattice potential  $V(\mathbf{r}) = (U_0/2) \cos(2k_r x)$  periodically modulates the condensate density  $\rho(\mathbf{r}) = |\psi(\mathbf{r})|^2$  with unit cell (UC) size

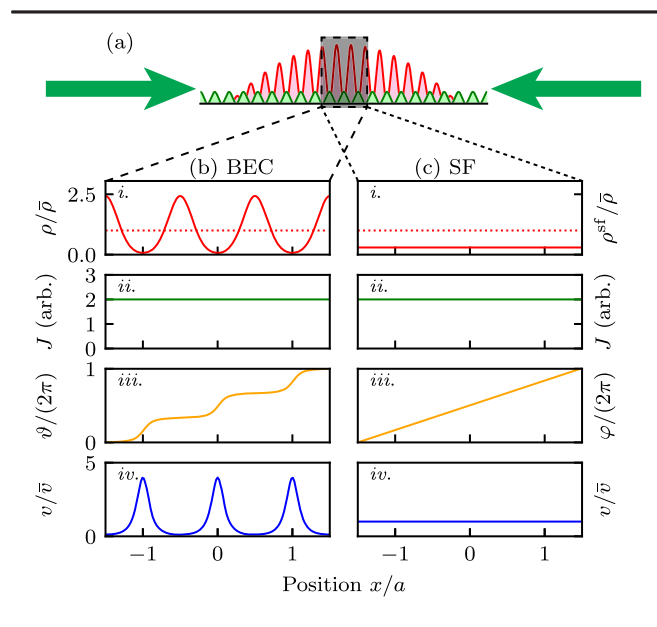


FIG. 1. Concept. (a) A BEC is confined in a harmonic trap superimposed with a 1D optical lattice (along  $\mathbf{e}_x$ , green), spatially modulating the condensate density (red). The dashed and dotted lines call out a region of nominally constant mean density and the left and right columns indicate the (b) state of the condensate and (c) SF in the presence of a current. These were computed for a  $5E_r$  deep lattice and plot: i. density (red), ii. current (green), iii. phase (orange), and iv. local velocity (blue). The red dashed line plots the mean density  $\bar{\rho}$ .

 $a = \pi/k_{\rm r}$  [Fig. 1(b) i]. By contrast, the SF order parameter  $\phi(\mathbf{r})$  is a coarse grained quantity describing system properties on a scale  $\gg a$ , giving the nominally uniform density in Fig. 1(c) i.

Even disregarding potential differences between  $\rho^{\rm sf}({\bf r})$  and  $\rho({\bf r})$ , we argue that  $\phi({\bf r})$  is not simply equal to  $\psi({\bf r})$  averaged over some scale large compared to a. The fundamental origin of this effect can be understood by considering a 1D system of size L with periodic boundary conditions in which both the condensate phase  $\theta$  and SF phase  $\varphi$  wind by an integer multiple N of  $2\pi$  [Figs. 1(b) and 1(c) ii], yielding a metastable quantized supercurrent [19]. To satisfy the steady-state continuity equation, the microscopic current  $J(x) = \rho(x) [\hbar \partial_x \theta(x)/m]$  must be independent of x [Fig. 1(b) ii], however, the periodically modulated density  $\rho(x) > 0$  implies the local velocity  $v(x) = \hbar \partial_x \theta(x)/m$  has oscillatory structure and consequently  $\theta(x)$  follows a staircase pattern [Fig. 1(b) iii, iv] with steps of height  $2\pi Na/L$ .

From macroscopic considerations the superfluid current is  $J = \rho^{\rm sf} [\hbar \partial_x \varphi(x)/m] = 2\pi N \hbar \rho^{\rm sf}/(mL)$ . Equating the currents obtained from the condensate wave function and the SF order parameter and integrating over a UC [20] yields Leggett's equation [6]

$$\rho^{\rm sf}(x) = \left[\frac{1}{a} \int_{\rm UC} \frac{dx'}{\rho(x+x')}\right]^{-1},\tag{1}$$

along with

$$\varphi(x) = \frac{1}{a} \int_{UC} \vartheta(x + x') dx'.$$

GPE simulations confirm that these analytical relations are valid independent of the lattice period to healing length ratio (see Supplemental Material [21] for a more rigorous derivation). Equation (1) further implies that  $\rho^{\rm sf} \leq \bar{\rho}$ , where  $\bar{\rho}$  is the spatial average of the condensate density over a UC, and at zero temperature the remaining density  $\rho^{\rm n} = \bar{\rho} - \rho^{\rm sf}$  behaves as a normal fluid pinned to the lattice potential.

In a 3D system, the current  $J_i = \rho_{ii}^{sf} [\hbar \partial_i \varphi/m]$  derives from an SF density tensor (having employed the Einstein summation convention). Provided that the condensate phase can be expressed as  $\vartheta(\mathbf{r}) = \vartheta_{r}(x) + \vartheta_{v}(y) + \vartheta_{z}(z)$ , the argument above in conjunction with the 3D continuity equation implies that  $\rho_{ii}^{sf}$  is diagonal, and the analogs to Eq. (1) for each of the three elements use the 1D density integrated along the transverse directions [25]. In the more general context where mean field theory [such as the Gross-Pitaveskii equation (GPE)] is inapplicable or the condensate phase cannot be separated as above, the Leggett expression for  $\rho^{\rm sf}$  is an upper bound for the SF density [6]; in later work Leggett also found a lower bound [26]. Using the Leggett expression, this implies that the superfluid density is only reduced along the direction of the optical lattice, so  $\rho_{yy}^{\text{sf}} = \rho_{zz}^{\text{sf}} = \bar{\rho}.$ 

Experiment.—We used <sup>87</sup>Rb BECs with  $N \approx 2 \times 10^5$ atoms in the  $|F=1, m_F=1\rangle$  hyperfine ground state. A 1064 nm trapping laser with an elliptical cross-section, traveling along e<sub>r</sub> provided strong vertical confinement with frequency  $\omega_z/(2\pi)=220$  Hz; the in-plane frequencies, from  $\omega_{x,v}/(2\pi)=(34,51)$  to (56,36) Hz, were optimized for our different experiments. We created a 1D optical lattice using a retroreflected  $\lambda = 532$  nm laser traveling along  $\mathbf{e}_x$ , giving an a=266 nm lattice period, comparable to the  $\xi = 170(20)$  nm minimum healing length. The optical lattice was linearly ramped on in 100 ms to a final depth  $\leq 10E_{\rm r}$ , with single photon recoil energy and momentum  $E_{\rm r} = \hbar^2 k_{\rm r}^2/(2m)$ , and  $\hbar k_{\rm r} = 2\pi \hbar/\lambda$ , respectively [27]. For Bragg experiments the final state was measured using resonant absorption imaging after a 15 ms time of flight (t.o.f.); scissors mode measurements were performed in situ using partial transfer absorption imaging [29].

Anisotropic speed of sound.—The speed of sound for diagonal  $\rho_{ij}^{\rm sf}$  obeys the hydrodynamic relation [30]  $c_i^2 = f_{ii}^{\rm sf}/(\kappa m)$  in terms of the compressibility  $\kappa = \bar{\rho}^{-1}(\partial \bar{\rho}/\partial \mu)$ , the chemical potential  $\mu$ , and with density reduced by the superfluid fractions  $f_{ij}^{\rm sf} = \rho_{ij}^{\rm sf}/\bar{\rho}$ . This reduces to the well-known value  $c^2 = \mu/m$  for an isotropic homogeneous system (See [21] for the full dispersion beyond the linear approximation). The sound speed ratio

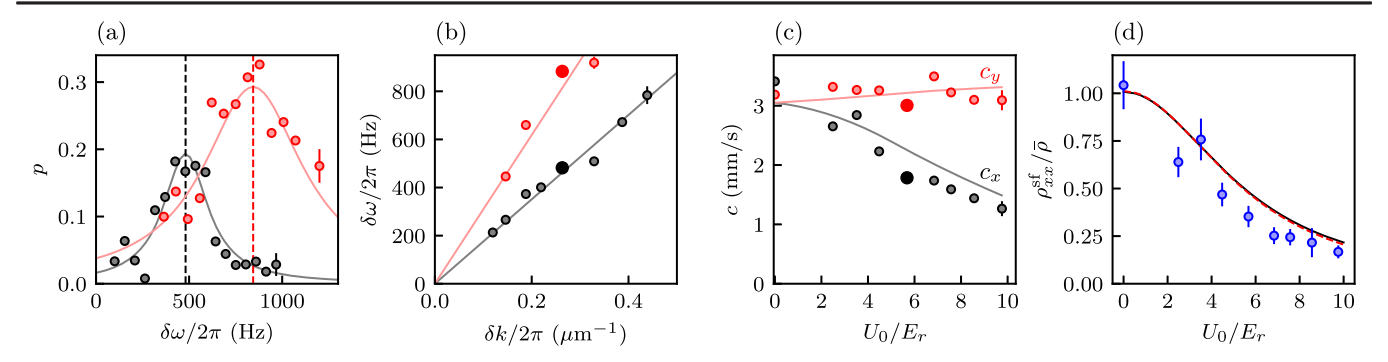


FIG. 2. Bragg spectroscopy. Black and red symbols mark excitations created along  $\mathbf{e}_x$  and  $\mathbf{e}_y$ , respectively. (a) Transferred population fraction p as a function of frequency difference  $\delta\omega$  with wave vector  $\delta k/2\pi=0.26~\mu\text{m}^{-1}$  and lattice depth  $U_0=5.7E_r$ . The solid curve is a Lorentzian fit giving the resonance frequency marked by the vertical dashed line. (b) Phonon dispersion obtained from Bragg spectra. The bold symbols resulted from (a) and the linear fit (with zero intercept) gives the speed of sound. (c) Anisotropic speed of sound. The bold symbols are derived from (b) and the solid curves are from BdG simulations (no free parameters [21]). (d) SF density obtained from speed of sound measurements (blue markers, error bars mark single-sigma statistical uncertainties). We compare with two models: the red dashed curve plots a homogeneous gas BdG calculation, and the solid black curve plots the result of Eq. (1). The simulations used our calibrated experimental parameters. In (a)–(c) each point has uncertainty as shown on the last point.

$$\frac{c_x^2}{c_y^2} = \frac{\rho_{xx}^{\text{sf}}}{\rho_{yy}^{\text{sf}}} = f_{xx}^{\text{sf}},\tag{2}$$

provides direct access to the different components of the superfluid density (see [21] for a Josephson sum rule argument). Because the density is y independent, Eq. (1) implies  $\rho_{yy}^{\rm sf} = \bar{\rho}$ .

We performed Bragg scattering using a weak sinusoidal potential with reciprocal lattice vector  $\delta k$  slowly moving with velocity v by patterning a laser beam with a digital micro-mirror device (DMD [31]) and measured the scattered fraction p. This results from what are effectively two interfering laser beams driving two-photon transitions with difference-wave vector  $\delta k$  and angular frequency  $\delta\omega = \delta k v$ . We applied this potential for  $\approx 5$  ms. Bragg transitions ensued when the difference energy and momentum were resonant with the BEC's Bogoliubov dispersion, and Fig. 2(a) shows data in the linear regime. The width of this spectral feature is limited by our BEC's inhomogeneous density profile; the resonance (vertical dashed line) obtained from a Lorentzian fit (solid curve) therefore reflects an average speed of sound [32]. The reduced Bragg signal at small  $\delta\omega$  results from the vanishing of the static structure factor in the phonon spectrum as  $\delta\omega$  goes to zero [33].

A series of such fits lead to phonon dispersion relations with Bragg-lattice period from 2.25 to 8.5  $\mu$ m. Representative dispersions taken along  $\mathbf{e}_x$  and  $\mathbf{e}_y$  are shown in Fig. 2(b), and we obtain the phonon speed of sound using linear fits. Figure 2(c) summarizes these data showing the speed of sound decreasing along the lattice direction  $\mathbf{e}_x$ , but slightly increasing along  $\mathbf{e}_y$  (resulting from the increased atomic density in the individual lattice sites). Finally, Fig. 2(d) shows our main result: the normalized superfluid density obtained from these data using Eq. (2) decreases as a function of  $U_0$ .

We compared these data to GPE simulations in two ways, we (i) used the Bogoliubov–de Gennes (BdG) equations [30] to obtain  $c_x$  and  $c_y$  and (ii) directly evaluated Eq. (1) from the GPE ground state density. The solid curves in Fig. 2(c) plot the sound speed obtained from solving the 1D BdG [34], and the red dashed curve in (d) is the ratio of these speeds. To compare with Leggett's prediction, we found the ground state of the 2D GPE for our experimental parameters and evaluated Eq. (1) throughout our inhomogeneous system. The black curve in (d) plots the resulting weighted average. Remarkably the BdG results are in near-perfect agreement with Leggett's expression.

Scissors mode.—The direct connection between the SF phase gradient and the velocity field greatly impacts rotational properties such as the moment of inertia I. For a highly anisotropic harmonic trap, the scissors mode [17,18] describes a fixed density distribution pivoting by a small angle  $\theta$  about an axis traversing trap center with frequency  $\omega_{\rm sc}$ . Scissors mode experiments are in spirit reminiscent of, though different in detail from, torsional balance experiments in  ${}^4{\rm He}$ , which give access to the nonclassical rotational inertia [8,9].

We describe the scissors mode in terms of the angular momentum density,

$$\Pi_{z} = m(xJ_{v} - yJ_{x}) = \hbar \bar{\rho}(xf_{vv}^{sf}\partial_{v}\varphi - yf_{xx}^{sf}\partial_{x}\varphi), \quad (3)$$

of the initial density distribution  $\bar{\rho}(\mathbf{r})$  oscillating by a small angle  $\theta(t)$ . Integrating  $\Pi_z$  over the system yields the total angular momentum  $L_z$ , then taking the derivative with respect to time gives the torque

$$\tau = \int d^3 \mathbf{r} \partial_t \Pi_z = -g \int d^3 \mathbf{r} \bar{\rho} [x f_{yy}^{sf} \partial_y \delta \rho - y f_{xx}^{sf} \partial_x \delta \rho],$$

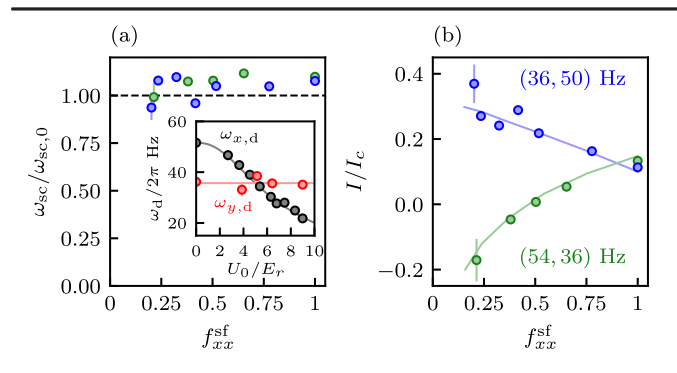


FIG. 3. Moment of inertia from scissors mode. (a),inset Measured dipole mode frequencies (circles) along with fits (curves) where the bare trap frequency is the only free parameter for each curve. (a) Normalized scissors mode frequency. Blue and green correspond to  $U_0=0$  trap frequencies (34,51) and (54,36) Hz, respectively. (b) Moment of inertia in units of  $I_{\rm c}$ . In (a) and (b) each point has uncertainty as shown on the first point. Symbols are the data computed as described in the text, and the solid curves are GPE predictions.

where g is the GPE interaction strength, and we used the linearized long-wavelength hydrodynamic kinetic equation  $0 = \hbar \partial_t \varphi + g \delta \rho$  to describe small changes in the density  $\delta \rho$ . Assuming an initial Thomas-Fermi distribution for  $\bar{\rho}$ , the small- $\theta$  density difference  $\delta \rho \approx -m\theta(\omega_x^2 - \omega_y^2)xy/g$  gives the torque

$$\tau = \frac{m\theta}{N} (\omega_x^2 - \omega_y^2) (\langle x^2 \rangle f_{yy}^{sf} - \langle y^2 \rangle f_{xx}^{sf}). \tag{4}$$

In this case, the equation of motion  $\tau = I\ddot{\theta}$  describes the scissors mode oscillations and thus connects the scissors mode frequency  $\omega_{\rm sc}$  to the moment of inertia

$$\frac{I}{I_c} = \frac{(\omega_x^2 - \omega_y^2)(\omega_x^2 f_{xx}^{sf} - \omega_y^2 f_{yy}^{sf})}{\omega_{sc}^2(\omega_x^2 + \omega_y^2)}$$
(5)

in terms of the classical moment of inertia  $I_c$ . This expression is in agreement with Ref. [17] when  $f_{xx}^{\rm sf} = f_{yy}^{\rm sf} = 1$ . Therefore we expect  $\omega_{\rm sc}$ , in conjunction with the superfluid density will give  $I/I_c$  as a function of lattice depth.

The inset to Fig. 3(a) plots the observed dipole mode frequencies  $\omega_{x,d}$  and  $\omega_{y,d}$  for a trap with bare (i.e.,  $U_0=0$ ) frequencies  $(\omega_x, \omega_y) = (54, 36)$  Hz. The dipole frequency  $\omega_{x,d}$  decreases with increasing  $U_0$ ; similarly to the sound speed, this is related to  $\rho^{\rm sf}$  via  $f^{\rm sf} = (\omega_{x,d}/\omega_x)^2$  along the lattice direction [21]. This ratio can also be expressed in terms of an increased effective mass  $m^*$ , with  $f^{\rm sf} = m/m^*$  [35]; this converges to the predictions of single-particle band structure [36] when the lattice period falls below the healing length; in our case the value computed

perturbatively from the GPE differs by about 20% from the band structure prediction. The result of this modeling is shown by the solid curves.

We excited the scissors mode using our DMD to tilt the harmonic potential by 50 to 140 mrad for  $\approx 1$  ms (shorter than the trap periods) and let the BEC evolve in the original trap for a variable time. We measured the resulting dynamics in situ and extracted the angle by fitting the resulting density profile to a rotated Gaussian. Figure 3(a) shows the scissors mode frequency normalized to the expected frequency [7] of  $\omega_{\text{sc},0}^2 = f_{xx}^{\text{sf}} \omega_x^2 + f_{yy}^{\text{sf}} \omega_y^2$  for a trap elongated either along  $\mathbf{e}_x$  [with frequencies (56,36) Hz, blue] or along  $\mathbf{e}_y$  [with frequencies (36,50) Hz, green]. In both cases  $\omega_{\text{sc}}$  appears to be about 5% in excess of the simple prediction, perhaps from finite temperature or anharmonicities in the optical dipole trap.

We combine these observations in Fig. 3(b) to obtain  $I/I_c$ ; the data (symbols) and our 2D GPE simulations (curves, with moment of inertia computed using  $I = \lim_{\Omega \to 0} \partial_{\Omega} L_z$ , with angular frequency  $\Omega = \dot{\theta}$ ) are in agreement [37]. For traps elongated along  $\mathbf{e}_x$  (green)  $I/I_c$  surprisingly changes sign when  $\omega_{x,d} = \omega_{y,d}$ . To understand the physical origin of this effect we now turn our attention to rotating systems.

Rotation.—Our discussion so far has focused on the superfluid density, and avoided questions about any associated normal fluid flow. We can deduce the existence of a normal fluid component by considering two thought experiments each a 1D ring geometry (with radius R) and in each case consider the resulting angular momentum. In case (i), we consider a lattice along the azimuthal direction that is very slowly accelerated [38] to a final angular velocity  $\Omega$ ; this is best understood by transforming into the frame corotating with the lattice. This leads to a lab frame angular momentum  $L_z/\hbar = 2\pi R(\bar{\rho} - \rho^{\rm sf})$  which we interpret as resulting from the normal fluid comoving with the lattice. In case (ii), we consider a complementary configuration with a static lattice and slowly insert a single quantum of "synthetic" magnetic flux (see Ref. [39] for a proposal using artificial gauge fields to provide synthetic magnetic flux). The process is equivalent to imprinting a  $2\pi$  phase winding (of the type discussed on page 1), giving angular velocity  $\Omega = \hbar/(mR^2)$  and angular momentum  $L_z/\hbar = 2\pi R \rho^{\rm sf}$ .

The Supplemental Material [21] confirms this picture of the existence of a normal fluid using 2D numerical simulations of rotating trapped systems with a 1D lattice where (i) the lattice corotates with the confining potential, or (ii) it is static in the lab frame (as in scissors mode experiments). In (i), the current results from a sum of normal and superfluid flow. The former corotates with the lattice and the trap, while the latter derives from the SF phase gradient. In (ii) there is no normal fluid flow, but as with our scissors mode observations,  $I/I_c$  changes sign.

Discussion and outlook.—In light of the discussion following Eq. (5), we cannot obtain  $I/I_c$  from scissors

mode measurements without detailed modeling, a conclusion that reinforces similar findings in supersolid dipolar gases [40]. (In that case, the degrees of freedom describing the droplet configuration can couple to scissors mode oscillations.) Reference [40] concluded that the scissors mode does directly yield the moment of inertia when 1D density modulations comove with the oscillatory motion: this is consistent with our findings comparing motion in static and rotating lattices. Although we conclude that a normal fluid exists, it is inseparable from the optical lattice and lacks any internal dynamics of its own, i.e., it is not described by a dynamical equation of motion. Similarly, calculations for the strongly interacting superfluid <sup>4</sup>He films on materials such as hexagonal boron nitride also predict an anisotropically reduced SF density [41], implying the existence of a pinned normal fluid.

In contrast, both the superstripe phase in spin-orbit coupled BECs [42–46] and supersolid phases of dipolar gases [13,47–49], support dynamical density modulations. Leggett's expression [Eq. (1)] applies to both of these systems implying a reduced superfluid density; in this case the associated normal fluid might exhibit dynamics, as expected for a conventional two-fluid model [17,18]. This leaves open questions regarding the nature of the normal fluid in the superstripe phase of spin-orbit coupled systems where an interplay between single-particle physics and interactions govern supersolidlike properties [50]. In addition,  $\rho^{\rm sf}$  is expected to be reduced outside of the superstripe phase [45,46] where the density is uniform (making Leggett's expression inapplicable), but the BEC's spin vector is spatially periodic.

*Note added.*—Recently, we become aware of a related work, using a 1D lattice with period longer than the healing length applied to a homogeneously confined 2D BEC [35].

The authors thank S. Stringari for suggesting this line of investigation and to both S. Stringari and S. Roccuzzo for stimulating discussions, and S. Mukherjee and W.D. Phillips for carefully reading the manuscript. This work was partially supported by the National Institute of Standards and Technology, and the National Science Foundation through the Physics Frontier Center at the Joint Quantum Institute (PHY-1430094) and the Quantum Leap Challenge Institute for Robust Quantum Simulation (OMA-2120757).

- \*These two authors contributed equally.
- J. R. Ensher, D. S. Jin, M. R. Matthews, C. E. Wieman, and E. A. Cornell, Phys. Rev. Lett. 77, 4984 (1996).
- [2] F. Dalfovo, S. Giorgini, L. P. Pitaevskii, and S. Stringari, Rev. Mod. Phys. **71**, 463 (1999).
- [3] V. F. Sears, E. C. Svensson, P. Martel, and A. D. B. Woods, Phys. Rev. Lett. 49, 279 (1982).

- [4] V. L. Berezinskii, Sov. Phys. JETP 34, 610 (1972), http:// www.jetp.ras.ru/cgi-bin/e/index/r/61/3/p1144?a=list.
- [5] J. M. Kosterlitz and D. J. Thouless, J. Phys. C 6, 1181 (1973).
- [6] A. J. Leggett, Phys. Rev. Lett. 25, 1543 (1970).
- [7] L. Pitaevskii and S. Stringari, Bose-Einstein Condensation and Superfluidity (Oxford University Press, New York, 2016), Vol. 164.
- [8] E. L. Andronikashvili, Zh. Eksp. Teor. Fiz. 16, 780 (1946).
- [9] G. B. Hess and W. M. Fairbank, Phys. Rev. Lett. 19, 216 (1967).
- [10] M. Boninsegni and N. V. Prokof'ev, Rev. Mod. Phys. 84, 759 (2012).
- [11] L. Tanzi, J. Maloberti, G. Biagioni, A. Fioretti, C. Gabbanini, and G. Modugno, Science 371, 1162 (2021).
- [12] M. A. Norcia, C. Politi, L. Klaus, E. Poli, M. Sohmen, M. J. Mark, R. N. Bisset, L. Santos, and F. Ferlaino, Nature (London) 596, 357 (2021).
- [13] F. Böttcher, J.-N. Schmidt, M. Wenzel, J. Hertkorn, M. Guo, T. Langen, and T. Pfau, Phys. Rev. X 9, 011051 (2019).
- [14] M. P. A. Fisher, P. B. Weichman, G. Grinstein, and D. S. Fisher, Phys. Rev. B 40, 546 (1989).
- [15] M. Greiner, O. Mandel, T. Esslinger, T. W. Hänsch, and I. Bloch, Nature (London) 415, 39 (2002).
- [16] M. Kozuma, L. Deng, E. W. Hagley, J. Wen, R. Lutwak, K. Helmerson, S. L. Rolston, and W. D. Phillips, Phys. Rev. Lett. 82, 871 (1999).
- [17] D. Guéry-Odelin and S. Stringari, Phys. Rev. Lett. 83, 4452 (1999).
- [18] O. M. Maragò, S. A. Hopkins, J. Arlt, E. Hodby, G. Hechenblaikner, and C. J. Foot, Phys. Rev. Lett. 84, 2056 (2000).
- [19] M. E. Fisher, M. N. Barber, and D. Jasnow, Phys. Rev. A 8, 1111 (1973).
- [20] Any average that removes the lattice structure suffices and the average over single UC where x' ranges from 0 to L is the most compact possible.
- [21] See Supplemental Material at http://link.aps.org/ supplemental/10.1103/PhysRevLett.131.163401, which includes Refs. [22–24] for rigorous coarse-grain mapping to derive the SF density, hydrodynamic model and GPE simulations to analyze rotation, and the Josephson sum rule discussion.
- [22] M. Krämer, L. Pitaevskii, and S. Stringari, Phys. Rev. Lett. 88, 180404 (2002).
- [23] R. C. Clark and G. H. Derrick, *Mathematical Methods in Solid State and Superfluid Theory: Scottish Universities' Summer School* (Springer, New York, 2013).
- [24] C. A. Müller, Phys. Rev. A 91, 023602 (2015).
- [25] Time reversal symmetry is also necessary so that each component—such as  $\psi_x(x)$ —has no nodes and can be made real valued [26].
- [26] A. J. Leggett, J. Stat. Phys. 93, 927 (1998).
- [27] We calibrated the lattice depth  $U_0$  by suddenly applying the lattice potential and fitting the resulting Kaptiza-Dirac scattering [28].
- [28] J. H. Huckans, I. B. Spielman, B. L. Tolra, W. D. Phillips, and J. V. Porto, Phys. Rev. A 80, 043609 (2009).
- [29] A. Ramanathan, S. R. Muniz, K. C. Wright, R. P. Anderson, W. D. Phillips, K. Helmerson, and G. K. Campbell, Rev. Sci. Instrum. 83, 083119 (2012).

- [30] L. Pitaevsiii and S. Stringari, Bose-Einstein Condensation (Clarendon Press, Oxford, 2003).
- [31] L.-C. Ha, L. W. Clark, C. V. Parker, B. M. Anderson, and C. Chin, Phys. Rev. Lett. 114, 055301 (2015).
- [32] In high-elongated quasi-1D BECs, the longitudinal speed of sound is reduced by a factor of  $\sqrt{2}$  from  $\sqrt{\mu/m}$ . We expect a related reduction from our tight confinement along  $\mathbf{e}_z$ , but for the Bragg spectra to exhibit inhomogeneous broadening from the nearly isotropic Thomas-Fermi profile in the  $\mathbf{e}_x$ - $\mathbf{e}_y$  plane.
- [33] J. Steinhauer, R. Ozeri, N. Katz, and N. Davidson, Phys. Rev. Lett. 88, 120407 (2002).
- [34] To make *k* a good quantum number we modeled untrapped systems with periodic boundary conditions. The chemical potential was selected to give the observed 3 mm/s speed of sound without the lattice present.
- [35] G. Chauveau, C. Maury, F. Rabec, C. Heintze, G. Brochier, S. Nascimbene, J. Dalibard, J. Beugnon, S. Roccuzzo, and S. Stringari, Phys. Rev. Lett. 130, 226003 (2023).
- [36] K. Jiménez-García and I. B. Spielman, *Annual Review of Cold Atoms and Molecules: Volume 2*, (World Scientific, New York, 2013), pp. 145–191.
- [37] Numerically we selected  $\Omega$  to be small enough that I did not depend on further changes in  $\Omega$ .
- [38] A. Browaeys, H. Häffner, C. McKenzie, S. L. Rolston, K. Helmerson, and W. D. Phillips, Phys. Rev. A 72, 053605 (2005).

- [39] N. R. Cooper and Z. Hadzibabic, Phys. Rev. Lett. 104, 030401 (2010).
- [40] S. M. Roccuzzo, A. Recati, and S. Stringari, Phys. Rev. A 105, 023316 (2022).
- [41] S. Moroni, F. Ancilotto, P.L. Silvestrelli, and L. Reatto, Phys. Rev. B 103, 174514 (2021).
- [42] Y. J. Lin, K. Jiménez-García, and I. B. Spielman, Nature (London) 471, 83 (2011).
- [43] J.-R. Li, J. Lee, W. Huang, S. Burchesky, B. Shteynas, F. Ç. Top, A. O. Jamison, and W. Ketterle, Nature (London) 543, 91 (2017).
- [44] Y. Li, G. I. Martone, L. P. Pitaevskii, and S. Stringari, Phys. Rev. Lett. **110**, 235302 (2013).
- [45] Y.-C. Zhang, Z.-Q. Yu, T. K. Ng, S. Zhang, L. Pitaevskii, and S. Stringari, Phys. Rev. A **94**, 033635 (2016).
- [46] G. I. Martone and S. Stringari, SciPost Phys. 11, 92 (2021).
- [47] L. Tanzi, E. Lucioni, F. Famà, J. Catani, A. Fioretti, C. Gabbanini, R. N. Bisset, L. Santos, and G. Modugno, Phys. Rev. Lett. 122, 130405 (2019).
- [48] L. Chomaz, D. Petter, P. Ilzhöfer, G. Natale, A. Trautmann, C. Politi, G. Durastante, R. M. W. van Bijnen, A. Patscheider, M. Sohmen, M. J. Mark, and F. Ferlaino, Phys. Rev. X 9, 021012 (2019).
- [49] M. Schmitt, M. Wenzel, F. Böttcher, I. Ferrier-Barbut, and T. Pfau, Nature (London) 539, 259 (2016).
- [50] A. Putra, F. Salces-Cárcoba, Y. Yue, S. Sugawa, and I. B. Spielman, Phys. Rev. Lett. 124, 053605 (2020).